Assessment of different methods for the prediction of marine propellers induced pressures

S. Gaggero, G. Tani, D. Villa & M. Viviani
Department of Electrical, Electronic, Telecommunication Engineering and Naval Architecture (DITEN), Genoa University, Genoa, Italy

F. Conti & C. Vaccaro
Fincantieri C.N.I. Naval Vessel Business Unit, Genoa, Italy

ABSTRACT: This paper addresses the problem of the prediction of propellers induced pressures; to this aim numerical and experimental results (both in model and full scale) in correspondence to different functioning conditions for a fast twin screw ship are reported. Numerical results were obtained by means of two different BEM codes and, only for specific cases, of a RANSE solver. Experiments were carried out both in model scale at cavitation tunnel and in full scale.

1 INTRODUCTION

The problem of marine propellers induced pressures has been treated for long time, both experimentally and numerically. Pressure pulses are one of the possible side effects of cavitation and, together with radiated noise, their limitation is becoming a mandatory requirement for high added value ships, such as cruise vessels, naval ships, mega yachts, for which the sole avoidance of erosive cavitation phenomena is far from being satisfactory.

Various methods to approach this problem have been proposed during years by different authors, ranging from potential flow solvers (lifting surface and panel codes) to more accurate and time demanding viscous codes (RANSE solvers). Among the different methods, various levels of approximations may be used, as an example considering the effect of the hull, completely representing it, or adopting some simplification. When the propeller functioning is highly non-stationary and the propeller works in cavitating regime, the accuracy of the various methods may become very different, with results that in some cases are not completely satisfactory.

This paper reports a comparison of different methods to assess pressure pulses of a propeller of a fast twin screw ship in correspondence to different functioning conditions, ranging from low speed with nearly no cavitation to higher speed for which cavitation is present. For this ship, measurements in model and in full scale are available. In section 2, the test case considered is briefly described, together with the setup adopted for the measurements. As it will be shown, the cavitation tunnel setup was very simple, with only inclined shaft and a flat plate instead of a complete hull. This setup, nearly mandatory for the Cavitation tunnel of the Genoa University due to the small dimensions of the facility, allows to assess the necessity of more complex configurations for this kind of ship by means of the comparison with full scale data. Moreover, being the configuration simplified, it represents an interesting case for the validation of numerical calculations, without requiring a too demanding setup.

Three different numerical methods have been considered for the prediction of pressure pulses.

In particular, two different panel codes were utilized, one developed in-house at Genoa University and the other currently available at Fincantieri. These codes, despite being simpler than viscous ones, present the great advantage of being considerably less computationally demanding. This allows their use in day-by-day activity during normal design processes. Moreover, with respect to the previously adopted lifting surface codes, they allow to obtain a better representation of the propeller and to capture all the 3D flow effects, improving considerably the accuracy of the results.

The results of the panel codes were also compared (in correspondence to one functioning condition only) to the correspondent ones obtained with the commercial solver StarCCM+. In this case, in order to reduce the complexity of the case, it was decided to reproduce the simpler configuration adopted at the cavitation tunnel. This allowed to keep the computational effort to reasonable levels, with the aim of a possible application for design activities.

A brief description of the codes adopted in this work is reported in section 3.

The results of the numerical simulations and the measurements are reported in section 4, including the propeller open water curves, the cavitation extents and the pressure pulses.

2 TEST CASE DESCRIPTION

The ship selected for this analysis is a fast twin screw / twin rudder ship.

The main characteristics of the ship are reported, in non-dimensional form, in Table 1; L is the ship length, B is the ship beam, T is draft and C_B is block coefficient. As a matter of fact and due to confidentiality reasons, it is not possible to provide complete data regarding the ship.

Table 1. Main characteristics of the ship.

L/B	7.5
B/T	3.25
$L/V^{1/3}$	7.1
C_B	0.5
Max F_N	Abt. 0.4

The ship is equipped with two 5 bladed controllable pitch propellers, whose characteristics are reported in Table 2, where $p_{0.7}$ and $c_{0.7}$ are the pitch and chord at 70% of the propeller radius, D is propeller diameter, A_E/A_O is the expanded area ratio, Z is the blade number. The configuration of the two propellers is inward over the top.

Table 2. Main characteristics of the propellers.

$p_{0.7}/D$	1.44
$c_{0.7}/D$	0.37
A_E/A_O	0.64
Z	5

As mentioned in the introduction, a series of experimental measurements, both in model and full scale, are available. These results have been compared with the numerical calculations for the assessment of their reliability. In the following paragraphs, a brief description of these tests is reported.

2.1 *Sea Trials measurements*

The sea trials have been carried out in correspondence to the ship design draught in calm sea. As usual during this kind of tests, ship speed has been progressively increased, covering the whole operating range, from rather low speed conditions to the maximum achievable speed. This allows considering conditions with very limited propeller cavitation and conditions with more developed cavitation, thus providing an interesting and ample test case for the various numerical codes adopted for pressure pulses predictions.

For each experiment the machinery setting (RPM and propeller pitch) are the mean of data from the two shaft lines.

For what regards the pressure pulses measurements, they have been carried out adopting the sensors PCB 106B50, which have been located in the hull above the propeller position. A schematic drawing of the sensors positions onboard is reported in Figure 1.

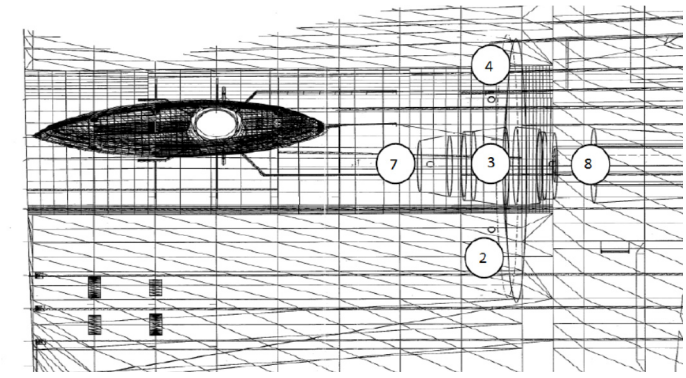

Figure 1: Pressure sensors positions during sea trials

As it can be seen, three sensors are located in correspondence to the propeller disk, namely sensor 3 (above the tip at 12 o'clock position) and sensors 2 and 4 at about one radius distance from the shaft line towards the ship center line and the ship side respectively. Other two sensors are aligned with sensor 3 and shifted longitudinally aft (sensor 7) and fore (sensor 8).

Actually, other sensors were present onboard the ship, but the ones mentioned have been considered for the present work since they are more significant from the point of view of propeller induced pressures.

For the present work, four different functioning conditions have been considered, as summarized in Table 3, where V_S is the ship speed, K_T is the thrust coefficient, σ_N is the cavitation number based on propeller revolutions. For the sake of confidentiality, all data are reported as a percentage of the value at maximum speed considered.

Table 3. Functioning conditions during sea trials.

Condition	V_S	K_T	σ_N
1	56%	76%	343%
2	64%	84%	244%
3	95%	88%	106%
4	100%	100%	100%

Observing the table, it is clear that the four conditions may be grouped in pairs, i.e. two moderate speeds (conditions 1 and 2) and two high speeds (conditions 3 and 4). In all cases, the increment of speed leads, as usual for this kind of ship, to an increase of the propeller loading and, obviously, to a decrease of the cavitation number.

For what regards propeller cavitation, as discussed also in sub-section 4.2, the first two conditions are characterized by the sole presence of tip vortex (near inception for condition 1, more developed in condition 2), while in conditions 3 and 4 also back side sheet cavitation is present, together with a rather strong tip vortex.

2.2 *Cavitation tunnel setup*

In this section results of model scale measurement are reported.

Cavitation tunnel tests have been carried out at the University of Genoa cavitation tunnel which is a Kempf & Remmers closed water circuit tunnel with a squared testing section of 0.57 m x 0.57 m, having a total length of 2 m.

The tunnel is equipped with a Kempf & Remmers H39 dynamometer, which measures the propeller thrust, the torque and the rate of revolution. As usual, a mobile stroboscopic system allows to visualize cavitation phenomena on the propeller blades. Moreover, cavitation phenomena visualization in the testing section is also made with three Allied Vision Tech Marlin F145B2 Firewire Cameras, with a resolution of 1392 x 1040 pixels and a frame rate up to 10 fps.

As usual for twin screw vessel propeller inflow is modelled at cavitation tunnel simply by means of shaft inclination. This, according to ITTC 2014 recommended procedures, is the standard setup for twin-screw vessels when it is not possible to install the hull model in the test section, as in present case.

Actually, it is common practice for this kind of ships to install also the main shaft line appendages (shaft brackets) in order to reproduce their influence on the propeller inflow. However, in this case they were not adopted in order to further simplify the test case.

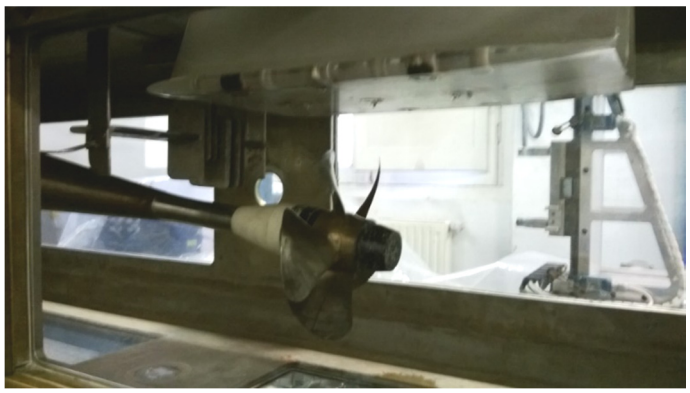

Figure 2: Cavitation tunnel setup

In addition a flat plate with faired leading and trailing edges is located over the propeller.

This element is the pressure sensors housing and is aimed to model (partially, of course) the presence of the aft part of the hull above the propeller, where pressure fluctuations are measured.

The distance between the plate and the propeller tip reproduces the clearance between the propeller and the hull.

The setup configuration at the tunnel is visible in Figure 2. Actually, in the figure also further elements are visible, i.e. flat plates upstream the propeller which were used to stimulate a different ship wake; these elements were eliminated in the present campaign, in order to maintain only the inclined shaft.

Five Kulite XTL-190M-5G differential pressure transducers are adopted for pressure pulse measurement. Sensors positions with respect to the propeller are given in Figure 3; in the table, for the sake of simplicity, same numbers as used during the sea trials are adopted.

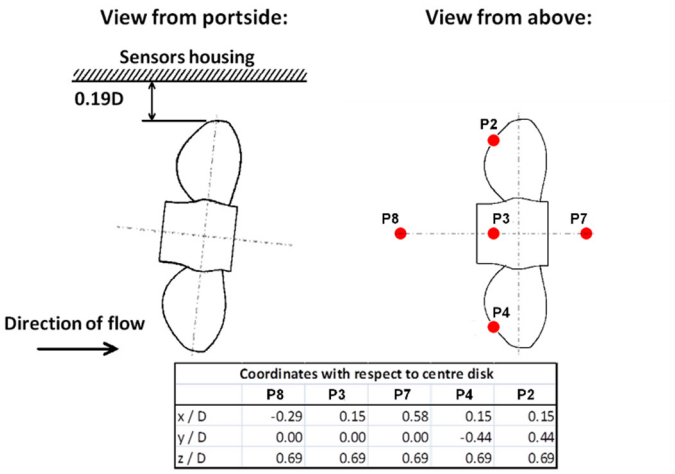

Coordinates with respect to centre disk					
	P8	P3	P7	P4	P2
x / D	-0.29	0.15	0.58	0.15	0.15
y / D	0.00	0.00	0.00	-0.44	0.44
z / D	0.69	0.69	0.69	0.69	0.69

Figure 3: Pressure sensors positions at cavitation tunnel

UNIGE cavitation tunnel is also equipped with an oxygen sensor used as an indication of the total amount of gas dissolved in water. In this case, cavitation tests are carried out at an oxygen content such to have $\alpha/\alpha_S = 0.5$ in standard temperature and pressure conditions, where α and αs represent actual and saturation oxygen content respectively. This resulted in a dissolved oxygen value of about 4.5ppm.

The tests carried out in present campaign are open water tests (in order to verify correspondence with towing tank results), cavitation extent observations and induced pressure measurements. In the latter, sensors signals are acquired simultaneously with the trigger signal of the dynamometer. This allows to compute the ensemble average of propeller revolution. The main advantage of the ensemble average is to preserve only the deterministic parts of the signal, removing by averages in the time domain random fluctuations. The harmonic analysis of the resultant signal gives the amplitudes and phases of tonal components of the pressure pulses.

Results are then given in non-dimensional form, using the pressure coefficient K_P, defined as:

$$K_P = \frac{p}{\rho N^2 D^2} \tag{1}$$

where p is the amplitude of the tonal component, N are propeller revolutions and ρ is water density.

Propeller operational conditions for cavitation tunnel tests are usually defined following the similarity of thrust coefficient and cavitation index.

The cavitation index similarity does not imply necessarily that cavitation phenomena are correctly modelled at the cavitation tunnel, because of scale effects.

Actually the inception of tip vortex cavitation depends on the Reynolds number following the law de-

fined by McCormick (1962). This means that in general tip vortex cavitation at cavitation tunnel occurs at a cavitation index significantly lower than inception index in full scale.

Consequently, the adoption of cavitation number similarity is valid only for operational conditions characterized by well-developed vortex cavitation while it leads to inconsistent results when applied to close to inception conditions.

In such cases, different similarity laws should be considered. In particular, this is the case of conditions 1 and 2 of present work. In accordance with the previous discussion, cavitation tunnel operational conditions corresponding to conditions 1 and 2 were defined following the similarity of the ratio σ_i/σ where σ is the cavitation number and σ_i the inception number. This similarity is achieved scaling ship cavitation number according to the McCormick scaling law.

3 NUMERICAL TOOLS

In present section, the CFD codes adopted for the evaluation of propeller performances, and in particular of the resultant pressure pulses, are reported.

3.1 *Boundary Element Methods*

Unsteady propeller pressures and hull-induced pressures have been calculated by using two potential based Boundary element method (BEM), one developed at the University of Genoa (Bertetta et al. 2012, Gaggero et al. 2014a, Gaggero et al. 2010), the other available in Fincantieri.

The Boundary element method solves the Laplace equation for the perturbation potential $\phi(\boldsymbol{x})$, which replaces continuity under the hypotheses of incompressible, irrotational and inviscid flow, by a superposition of sources and dipoles distributed over the boundaries of the computational domain. As usual, the kinematic and the Kutta conditions allow solving the linear system of equations (one for each point on which the boundary condition itself is forced) that originates from the discretization of the "wetted" boundary surfaces (blades, hub and trailing wakes) via quadrilateral hyperboloidal panels. The computed strengths of the singularities represent the values of the perturbation potential and of its derivatives that, in turns, allow calculating pressure (and forces) through the Bernoulli theorem. Dedicated kinematic, dynamic and cavity closure boundary conditions, via an iterative approach, allow taking into account also the presence of a sheet cavity bubble on both suction and pressure side of the blade (Fine and Kinnas, 1993). For the partially cavitating propeller problem, the perturbation potential on any points $\boldsymbol{x}_p$ in the computational domain can be calculated by using equation (2) where S, S_c and S_w represent, respectively, the fully wetted part, the cavitating part and the trailing wake surfaces of the blades and of the hub. ϕ_{wake} is the potential jump on the vortical wake while $\boldsymbol{n}$ and $\boldsymbol{r}_{pq}$ stand for the local surface normal and the distance between the integration $\boldsymbol{x}_q$ and the influence $\boldsymbol{x}_p$ points. k is a constant depending by the position (in the domain or on its boundaries) of the influence point.

$$k\pi\phi(\boldsymbol{x}_p) = \int_{S+S_c} \phi(\boldsymbol{x}_q)\frac{\partial}{\partial \boldsymbol{n}_q}\frac{1}{\boldsymbol{r}_{pq}}dS - \int_{S+S_c} \frac{\partial\phi(\boldsymbol{x}_q)}{\partial \boldsymbol{n}_q}\frac{1}{\boldsymbol{r}_{pq}}dS + \int_{S_W} \phi_{wake}(\boldsymbol{x}_q)\frac{\partial}{\partial \boldsymbol{n}_q}\frac{1}{\boldsymbol{r}_{pq}}dS \quad (2)$$

The unsteadiness due to the non-homogeneous inflow is included directly into the kinematic boundary condition and it is driven by the Kelvin theorem through the numerical approach proposed by Hsin (1990). The axial symmetry of the problem is exploited to reduce the computational domain: only the key blade, indeed, is solved while the other are taken into account iteratively.

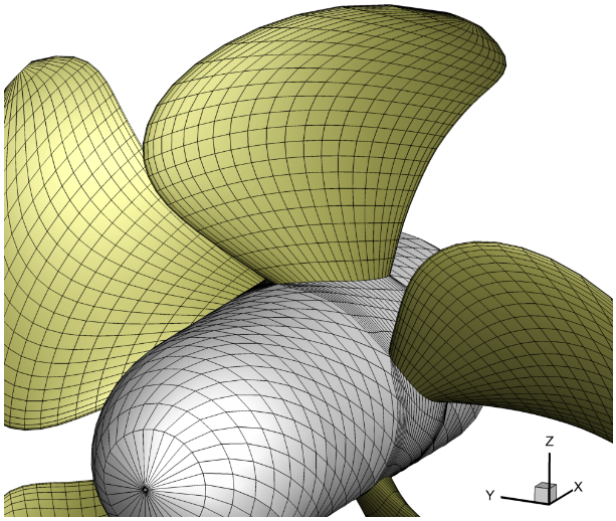

Figure 4: Surface mesh for BEM calculations – University of Genoa Boundary element method

The computational mesh consists, for both the adopted codes, in about two thousands panels per blade, distributed by using appropriate spacing at both leading and trailing edge. Unsteady calculations were carried out with an equivalent time step of 6° and six complete propeller revolutions were considered in order to achieve a periodic solution. Calculations performed with the Boundary element method developed at the University of Genoa were carried out by using an iterative (pressure) formulation of the Kutta condition at the blades trailing edge. With the Boundary element method available in Fincantieri, the simpler linear Morino (Morino and Kuo, 1974) implementation of the Kutta condition was preferred.

A discretization of the hull stern surface similar to that employed for the propeller blades was adopted in order to predict the induced pressure pulses by a slightly modified version of equation (2) in order to account for the mutual interactions between the hull and the propeller itself. An example of the computational mesh is shown in Figure 4.

3.2 *RANS code*

The viscous code has been applied only for the cavitation tunnel configuration, i.e. inclined shaft without any wake. With respect to the traditional propeller simulations, where an open field has been considered as external boundary, herein also the tunnel and all the features of the experimental setup have been included in the simulation domain, in order to include their effects on the propeller working point. The simulation has been carried out with thrust similarity with respect to experimental data. RANS equations have been solved for a homogeneous mixture with phase change in order to account for cavitation. By assuming the physical proprieties of the mixture as a weighted mean between pure liquid and vapor phases:

$$\begin{aligned} \rho_{mix} &= \gamma\rho_{vap} + (1-\gamma)\rho_{liq} \\ \mu_{mix} &= \gamma\mu_{vap} + (1-\gamma)\mu_{liq} \end{aligned} \tag{3}$$

where γ is the vapor volume fraction, the incompressible continuity and momentum equations for the mixture can be expressed as:

$$\begin{cases} \nabla \cdot \boldsymbol{u} = \left(\dfrac{1}{\rho_{liq}} - \dfrac{1}{\rho_{vap}}\right)\dot{m} \\ \dfrac{\partial \rho_{mix}\boldsymbol{u}}{\partial t} + \nabla \cdot (\rho_{mix}\boldsymbol{u}\boldsymbol{u}) = -\nabla p + \nabla \cdot \boldsymbol{T_{Re}} + \boldsymbol{S} \end{cases} \tag{4}$$

As usual $\boldsymbol{u}$ and p are the velocity and the pressure fields and $\boldsymbol{T_{Re}}$ is the tensor of Reynolds stresses, modeled through the Boussinesq eddy viscosity assumption in accordance to the turbulent closure equations (in present calculations the realizable $k-\varepsilon$ turbulence model). Additional momentum sources are included in $\boldsymbol{S}$. The system of equations (4) is closed by the additional equation that solves for the transport of the vapor volume fraction, through which the interaction between the vapor and the liquid phases is modeled:

$$\frac{\partial \gamma}{\partial t} + \nabla \cdot (\gamma \boldsymbol{u}) = \frac{\dot{m}}{\rho_{vap}} \tag{5}$$

In present calculations the net interphase mass flow rate per unit volume $\dot{m}$ has been calculated by using the Schnerr-Sauer approach (Schnerr and Sauer, 2000).

A sliding mesh approach has been used to take into account the relative motion of the propeller with respect to the tunnel and, following the best practice developed by the authors in previous works (Gaggero et al. 2014a, Gaggero et al. 2014b), a 5.2 million cells mesh has been used for the whole domain. Most of these (4.2 million) were used to accurately describe the propeller blades and their boundary layer (10 layers of cells for 2 mm of total prism layer thickness) with a minimum cell size of 0.05 mm and a mean value of 1.5 mm (in model scale). The remaining cells (about 1 million) were used to discretize all the upper part of the tunnel with particular attention for the region near the pressure transducers (with 0.5 mm as minimum cell size). In Figure 5 an extract of the used mesh is shown. As highlighted in Gaggero et al. (2014a) the time step plays an important role for the solution accuracy (in particular if cavitation is considered), for this reason a time step equivalent to 1° of blade revolution has been used to maintain the Courant number lower than 1 in the major part of the domain. The simulation ran for 1 week on a workstation (two processor Intel Xeon 2.60 GHz with 10 cores each) to simulate 10 propeller revolutions.

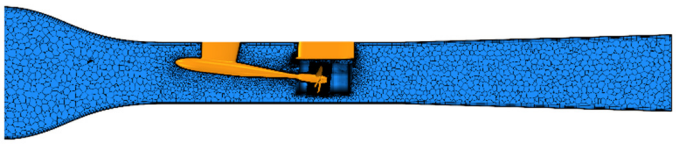

Figure 5: Mesh arrangement for RANSE calculations.

4 RESULTS AND DISCUSSION

4.1 *Open water propeller curve*

In this section, the numerical results for the propeller in open water conditions obtained by the BEM and RANS codes are summarized and compared with the experimental data available from towing tank tests. In Figure 6, all the data are made non-dimensional for confidentiality reasons. The accuracy of both the potential codes and the viscous code is noticeable and comparable with previous numerical results for other propellers (Gaggero et al. 2010).

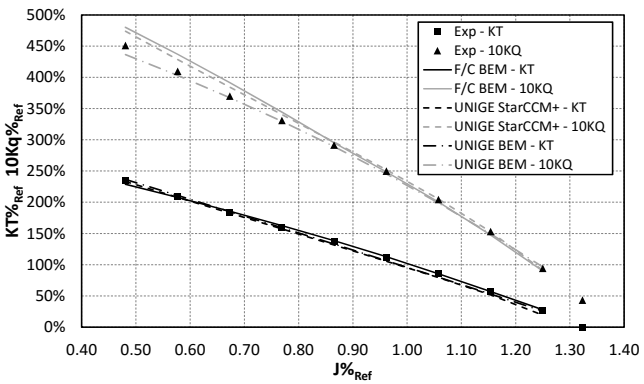

Figure 6: Propeller open water characteristics.

All codes present a slight underestimation of the thrust for high values of advance coefficient (J). On the contrary, the viscous and potential codes have a different behavior for the torque at low J values. At low advance coefficient, a rather good correspondence is also present, even if F/C BEM and RANS code tend to slightly overestimate thrust.

4.2 *Cavitation observations*

In this section, cavitation observations carried out at the cavitation tunnel are considered for comparison with numerical results and sea trials.

Only two functioning conditions are considered for the sake of shortness, condition 1 and condition 4.

As explained in sub-section 2.2, condition 1 has been defined for model tests scaling the cavitation number according to the McCormick law, resulting in a value lower than that used for numerical computations.

As visible in Figure 7, the propeller is not cavitating, except a very thin tip vortex (evidenced by the red circle) in the wake between 90° and 180° blades angular positions (0° corresponds to the 12 o'clock position).

For what regards condition 4, model scale cavitation observations have been carried out at a slightly higher cavitation number than that reported in table 3 (with an increment of about 10%).

The cavitation pattern, shown in Figure 8, consists also in this case, only in tip vortex cavitation in the wake between 90 and 180°, more developed with respect to condition 1.

Figure 7: Condition 1, model scale cavitation extensions.

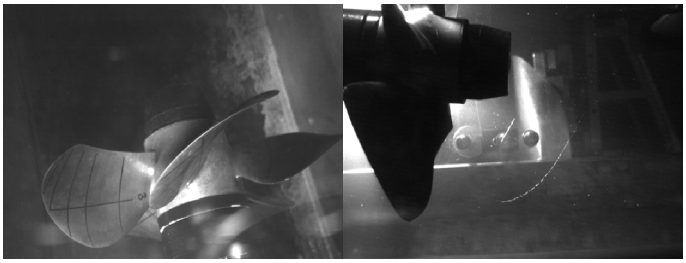

Figure 8: Condition 4, model scale cavitation extensions.

This cavitation extension is reasonably slightly underestimated because of the higher cavitation number. According to visual observations and inception tests, however, differences should be small and limited to the development of the tip vortex. Actually sheet cavitation occurs in model scale only in correspondence to a significantly lower value of the cavitation number; the cavitation index of condition 4 is very near to the inception index of suction side root bubbles at 90°.

It is important to remark that for conditions 3 and 4 cavitation observation were carried out also at full scale in order to check the risk of erosive cavitation. Unfortunately, photographs of full-scale cavitation patterns are not available; nevertheless, the visual observations excluded the presence of root bubbles in all conditions tested.

For what regards in general cavitation behaviour in full scale, cavitation extensions were larger than in model scale, resulting in a more developed tip vortex and sheet cavitation between 0° and 90° (rather small and very close to the tip for condition 3, more extended radially for condition 4).

These discrepancies with model scale tests are reasonably connected to different viscous scale effects. Actually for condition 4 the McCormick scaling of the operational cavitation number law was not considered being cavitation too much developed to adopt the σ_i/σ similarity. In addition, such similarity would result in an unrealistically low cavitation number in model scale.

On the other hand, due to the largely different Reynolds number, tip vortex cavitation in full scale should be somehow more developed and also sheet cavitation may be present, even if its inception does not follow strictly the McCormick law.

In addition it has to be remarked that model scale tests have been carried out considering only the inclined shaft, reproducing the vertical velocity components, and thus neglecting the axial wake components. However, some axial wake components may be present also in full scale, even if limited (mainly due to the presence of shaft brackets and shaft line wake and to a possible influence of the ship boundary layer in the upper part of the propeller disk).

This configuration is rather common for twin screw ships because of the limited extent and magnitude of the various above mentioned wake components, which become even smaller when moving to full scale because of the larger Reynolds number. However, assuming these flow disturbances to be negligible and completely eliminating their presence may partially lead to the observed underestimation of propeller cavitation.

Cavitation extensions, both in model scale with inclined shaft only and in full scale were also predicted by means of numerical calculations (namely UNIGE BEM and RANS codes for model scale case and both BEM codes for the full scale case).

For what regards the full scale calculations, the inflow wake measured at towing tank was used, thus considering a condition with a slightly more marked wake than it could be expected in reality. Actually the real ship wake field is probably intermediate between

the model scale wake field and the simplified assumption adopted at the cavitation tunnel.

In Figure 9, the results in correspondence to condition 4 in model scale tests (only shaft inclination) are reported.

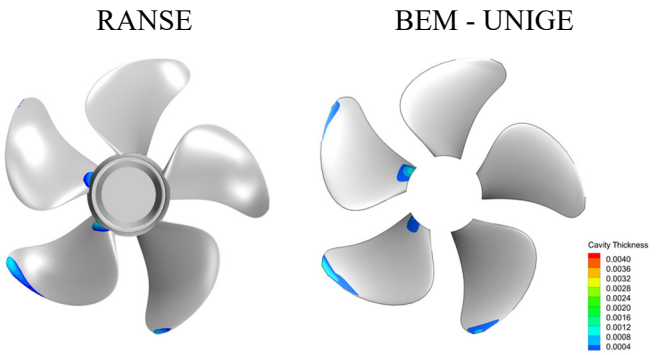

Figure 9: Model scale cavitation extensions predicted by RANS and BEM methods.

As it can be seen, results are in good agreement and cavitation extensions are generally very limited.

Cavitation extensions predicted by the BEM method are only slightly over estimated, with a thin strip of cavitating panels near to the tip between 90° and 180°, in good correlation with the presence of the tip vortex in the experiments. Also the few cavitating panel in correspondence to the blade root at 90° are in good agreement with the previously mentioned inception of bubble cavitation for condition 4 at cavitation tunnel.

Analogous cavitation pattern have been predicted with the RANSE solver, confirming the presence of tip vortex cavitation and root bubble cavitation (near inception) at 90°.

For what regards prediction at full scale, cavitation extensions predicted by the two BEM computations are compared in Figure 10 and Figure 11, for condition 1 and 4 respectively.

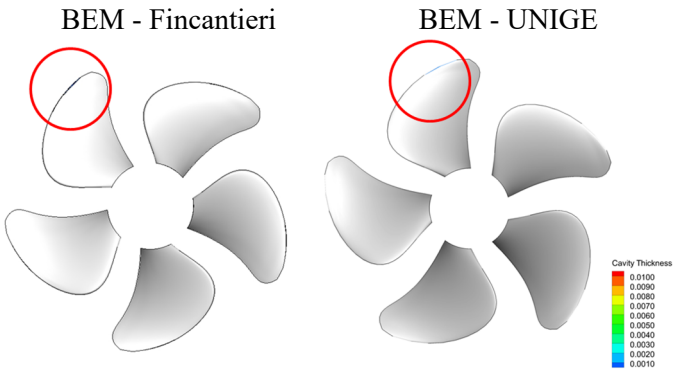

Figure 10: BEM cavitation extensions, ship case, condition 1.

For condition 1 cavitation is still almost not present, with the only exception of a very limited cavity near to the tip in correspondence to the wake peak (highlighted by the red circle in Figure 10). These few cavitating panels may be regarded as an indication of the possible presence of tip vortex cavitation whose prediction is beyond the capabilities of a normal boundary elements method.

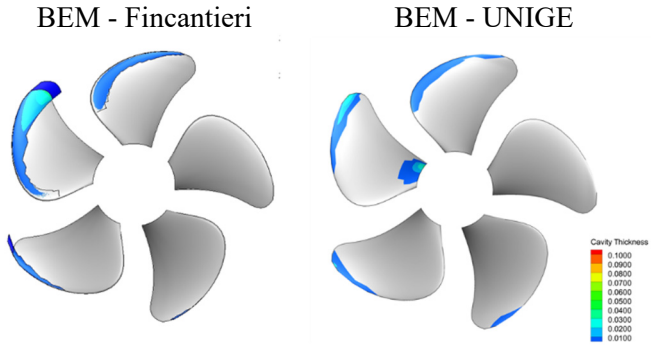

Figure 11: BEM cavitation extensions, ship case, condition 4.

Cavities reach their maximum extensions in correspondence to angular positions between 20° and 60°, where the wake is more intense. Cavities dimensions are only slightly reduced while moving toward the 90° position because of the combined effect of axial wake and inclined shaft, then sheet cavitation decreases, with only a small cavity close to the tip at 180°.

This cavitation pattern is qualitatively similar to what observed during sea trials but the extensions are increased, especially for what regards the code adopted by Fincantieri. However this is in rather good agreement with expectations, keeping in mind that the model scale wake field has been adopted for the BEM computations. As a consequence, as already pointed out, a more marked wake than in full scale has been adopted, overstimulating cavitation. It has to be pointed out, however, that the different wake is only a partial explanation for the higher cavitation extension, since, as mentioned, in full scale sheet cavitation was present, but very limited; in particular, in correspondence to 90° angular condition almost no cavitation was present (apart the tip vortex) in a position in which the effect of the axial wake is negligible. This underlines the fact that the predicted cavitation extent is probably slightly overestimated, even not considering the effect of the different wake.

These results stress the influence of propeller inflow on cavitation extension, even in the case of a twin screw vessel. These differences have an effect also on pressure pulses, as it will be shown in the following of this work. From this point of view the full scale data may shed some light on this problem.

4.3 *Pressure pulses*

In this section results of pressure pulses measurements carried out in model scale and full scale are compared with pressure fluctuations computed with numerical methods.

In this work, attention is focused only on the amplitude of the pressure fluctuations in correspondence to the blade passage frequency (1st blade harmonic).

At first, results of model scale tests are compared with full scale measurements. The similarity of the

pressure coefficient K_P is assumed between model scale and full scale. For each operational condition cavitation tunnel tests were performed also without tunnel depressurization, thus suppressing cavitation. Such conditions are considered too in order to better appreciate the effect of cavitation on pressure pulses, if present.

As it can be seen in Figure 12, there is a rather good agreement between model scale predictions and full-scale measurements.

In particular, results of cavitation tunnel experiments seem to correctly capture ship pressure pulses in correspondence to sensors 3, 4 and 7 while the agreement is slightly worse in the case of sensors 2 and 8.

Analysing all the operational conditions together it can be noticed that differences between model and full scale are almost always the same, independently of the ship speed. This suggests that the previously mentioned discrepancies in cavitation patterns between model and full scale are not the main causes of differences in measured pressure pulses.

Actually it has to be reminded that a flat plate was adopted in the cavitation tunnel instead of a hull model and, consequently, the pressure distribution on a plate may be different from that on the real hull, especially in the cases of lateral sensors (2 and 4) because of possible three-dimensional effects. Moreover, in the model test configuration the ship rudder is not present, being a further source of discrepancy between the two cases. The measured pressure fluctuations in terms of non-dimensional pressure coefficient show rather limited variations between considered operational conditions, despite they are significantly different in terms of both thrust coefficient and cavitation index (see table 3).

Actually, for what regards sea trials, the largest variation is observed in the case of sensor 2, condition 4, with an increment of about 60% with respect to other conditions. This may be due to the particular location of the transducer, above the position were the largest cavity extensions are present.

The effects of propeller load and cavitation number may be analysed separately only in the case of model tests. Focusing on cavitation tunnel results values seem almost constant, both with respect to the thrust coefficient (limiting to the tested values) and cavitation number.

For what regards the latter, in model scale the almost null contribution of cavitation is in line with the very limited cavitation extensions observed.

For what regards the propeller load, the low differences observed may be related to the particular propeller design, with rather low tip loading.

As already mentioned a certain extent of sheet cavitation was observed during sea trials for conditions 3 and 4, thus the limited effects on pressure pulses seem a bit surprising, even if it has to be remarked again that full scale cavitation was not very large.

As a general comment this first comparison between experimental results in model and full scale highlights the satisfactory capability of model scale experiments in predicting pressure pulses also in the case of small facilities with simplified configurations. A second aspect of great interest is the apparently low sensitivity of the pressure pulse first harmonic to cavitation, at least when cavity extensions are limited.

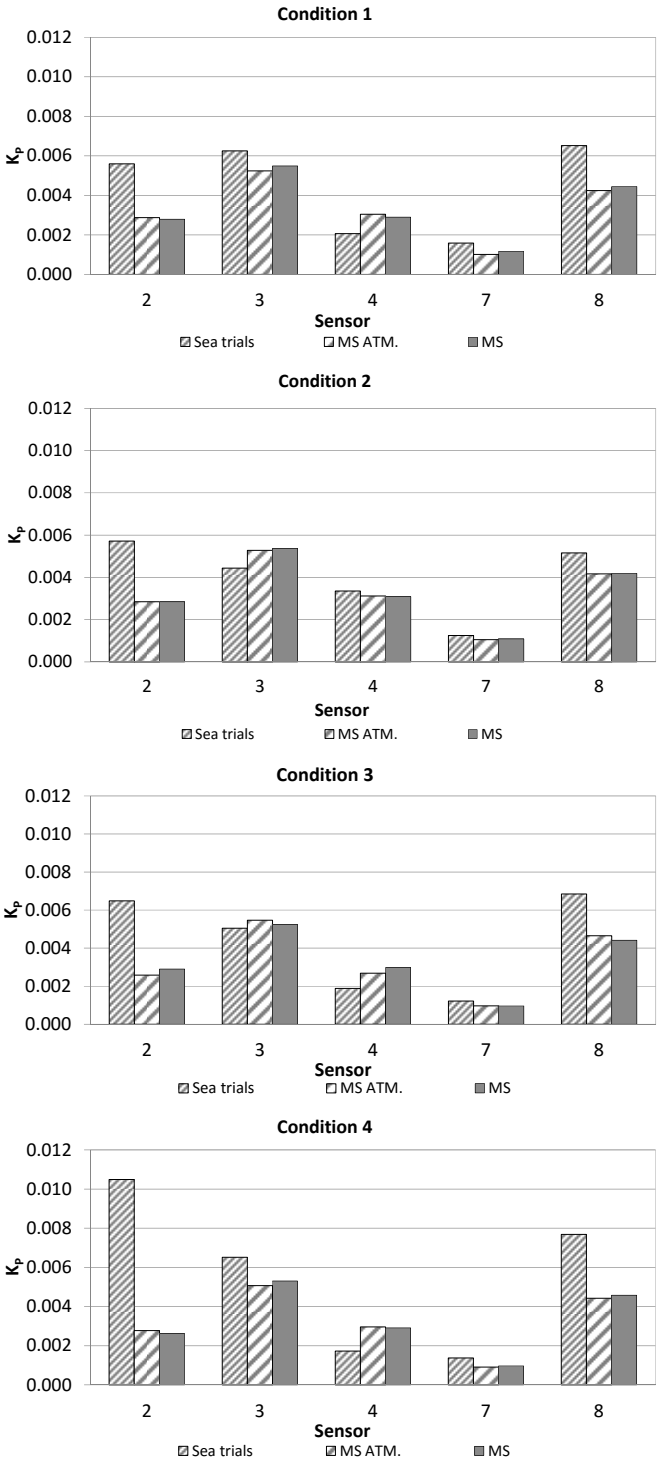

Figure 12: Full scale (Sea trials) and model scale non-cavitating (MS ATM) and cavitating (MS) pressure pulses.

This phenomenon, observed also in other cases (Kinnas et al. 2015) , should be further investigated, considering both model scale and full scale experiments and, if possible, cases with larger cavitation extension.

As a second comparison, pressure fluctuations computed with the panel methods are compared in Figure 13 with the sea trials results already discussed.

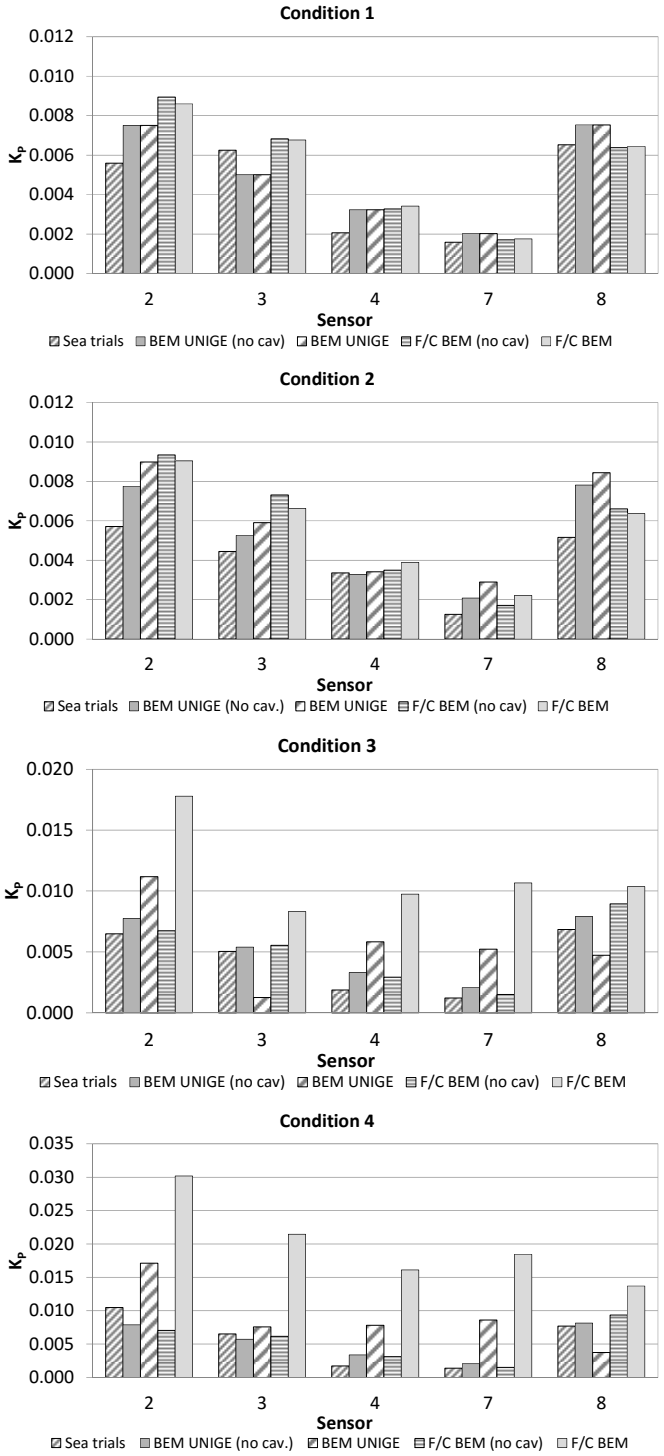

Figure 13: Pressure pulses predicted by BEM methods.

As it can be seen, as far as results of not cavitating computations are considered, the agreement between measurements and numerical prediction is remarkably good. However, considering computations in cavitating conditions, rather large discrepancies are observed for conditions 3 and 4. In particular for these conditions, because of the presence of suction side sheet cavitation, predicted pressure fluctuations amplitudes are increased by more than 100%, showing a behaviour remarkably different from the one observed for cavitation tunnel tests and sea trials.

This phenomenon may be partially due to the large cavity extensions predicted by the numerical codes because of the adoption of the model scale nominal wake field. However, considering that the numerically predicted cavitation extent is indeed not very large, it is believed that the effect of the cavities on the first harmonic of the pressure pulses is overestimated also for other reasons. This fact points out again the need to carry out ad hoc investigations on a suitable test case. These investigations should be carried out including both panel codes (as presently) and RANSE solvers, in order to analyse if the latter are more capable of avoiding pressure pulses overestimations. Such an activity might be carried out at first only comparing with model scale experiments, which may present two advantages.

First, at the cavitation tunnel a simpler configuration, such as the one adopted in present case, may be used, allowing to test numerical codes against a not too computationally demanding case; this would be very beneficial especially for testing RANSE codes, without the need of including in the simulation also the complete ship hull.

Moreover, in model scale considerably off-design conditions may be simply considered; in particular, tests could be carried out in correspondence to a high propeller loading, thus stimulating considerable cavitation extent, in order to analyse the capability of codes not only to capture cavity extensions but also to correctly evaluate the resultant pressure pulses.

A first step in this direction has been carried out simulating the model scale conditions with both RANSE and panel codes. However, as already remarked, the operational conditions considered at the moment are not suitable to clarify the discussed issue because of the limited cavitation in model scale. Notwithstanding this, the comparison of computed and measured pressure pulses, shown in Figure 14, is a useful preliminary indication of the reliability of employed models.

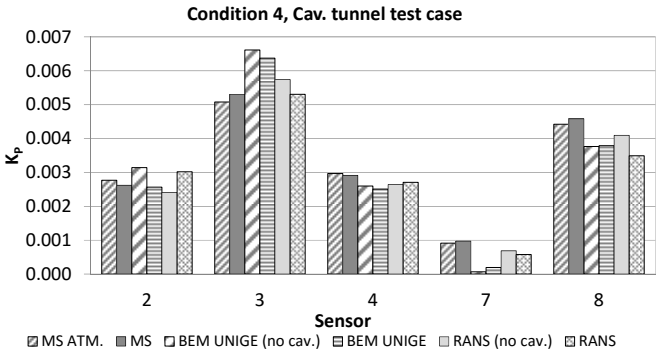

Figure 14: Cavitation tunnel test case3: experimental vs numerical pressure pulses.

As it can be seen the agreement between both numerical approaches and measurements is very good for all considered sensors, confirming the capabilities of these tools to predict propeller induced pressure

fluctuations in non-cavitating conditions or conditions with very limited cavitation extension.

As already remarked these results are not sufficient to clarify the problem of the overestimation of pressure pulses by the BEM codes when significant cavitation is present. However, this could be considered as the basis for further study on this topic.

5 CONCLUSIONS

In this work an extensive analysis of propeller cavitation and related pressure pulses for the case of a twin screw vessel has been presented.

The analysis included experimental measurements in both model scale and full scale, and numerical computations, mainly by means of BEM approaches. In addition, also a RANSE solver has been considered as a further tool for the investigation of propeller induced pressure fluctuations in cavitating conditions, limiting the attention to the simplified configuration at cavitation tunnel. The whole analysis allows highlighting some important aspects related to this topic.

First of all the comparisons between cavitation extensions observed at cavitation tunnel, during sea trials and predicted by BEM methods point out the significant effect of the hull wake on cavitation even in the case of a twin screw vessel, despite the limited hull wake.

Actually cavitation tunnel tests carried out neglecting the axial wake components are characterized by under-predicted cavitation if compared to full scale.

Anyway this simplified cavitation tunnel setup, largely adopted for twin screw vessels, allows to obtain reliable estimation of pressure pulses. This fact may be also partially explained by the fact that full scale cavitation patterns, even if larger than at cavitation tunnel, are still rather limited.

However it has to be remarked that this holds as far as only the first blade passage harmonic is considered, which is probably the less affected by cavitation.

Passing to the analysis of higher harmonics or of the broadband components a more accurate representation of the real hull wake is needed to enhance the similarity of cavitation patterns. On the other hand, the adoption of the model scale wake field as input for the panel methods brings to larger cavitation than in the real case. This fact may be partially responsible of the large overestimation of pressure pulses by BEM methods, when cavitation is considered in computations. However observed discrepancies seem not related only to the larger extensions but also to a certain tendency to overestimate the effect of cavitation on the first pressure pulse harmonic in panel methods.

Actually, it has to be remarked that considering only computations without cavitation (or with very limited cavitation) the agreement with experimental data is very good. To shed some light on this problem also viscous computations have been considered applied to the simpler cavitation tunnel test case. Calculations seem promising but, at the moment, the considered operational conditions are characterized by limited cavitation, not suitable to investigate the effect of large bubbles on the first pressure pulse harmonic. From this point of view, it could be useful to study, in model scale, operational conditions characterized by larger cavitation patterns, which may be obtained considering also the axial wake components or testing the propeller in off-design conditions, with higher loadings and consequently larger cavitation extents. Furthermore, the analysis should be extended also to higher order harmonics and to the broadband excitation.

As already mentioned, to this aim it is of utmost importance to consider cavitation tunnel configurations simulating as far as possible the three dimensional wake field expected in full scale. Moreover, it has to be remarked also that, while the prediction of the periodic pressure fluctuations from model scale measurements usually leads to acceptable results, the scaling of the broadband components may be significantly more difficult. The numerical prediction of these broadband components is rather challenging, with the need for significantly more complex and computationally demanding tools than BEM solvers.

6 ACKNOWLEDGEMENTS

This work has been partially funded in the context of the DLTM project “CLUSTER” (FAR-MIUR funds).

7 REFERENCES

Bertetta, D., Brizzolara, S., Gaggero, S., Viviani, M. and Savio, L. 2012: CP propeller cavitation and noise optimization at different pitches with panel code and validation by cavitation tunnel measurements, *Ocean Engineering* 53 pp. 177-195.

Fine, N.E. and Kinnas, S.A., 1993: A Boundary-Element Method for the Analysis of the Flow around 3-D Cavitating Hydrofoils, *Journal of Ship Research*, 37 (3), pp. 213-224.

Gaggero, S., Villa, D. and Viviani, M., 2014a: An investigation on the discrepancies between RANS and BEM approaches for the prediction of marine propeller unsteady performances in strongly non-homogeneous wakes, *Proceedings of the 33rd International Conference on Ocean, Offshore and Artic Engineering, OMAE 2014*, San Francisco, USA.

Gaggero, S., Tani, G., Viviani, M. and Conti, F., 2014b: A study on the numerical prediction of propellers cavitating tip vortex, *Ocean Engineering*, Volume 92 (2014b), pp. 137-161.

Gaggero, S., Villa, D., Brizzolara, S., 2010: RANS and Panel Methods for Unsteady Flow Propeller Analysis, *Journal of Hydrodynamics*, Ser. B, Volume 22, Issue 5, Supplement 1, pp. 564-569.

Hsin, C.Y., 1990: Development and analysis of Panel Methods for Propellers in Unsteady Flows, *PhD Thesis*, Massachusetts Institute of Technology.

ITTC – Recommended Procedures and Guidelines: Model scale noise measurements, 7.5-02-01-05, 2014

Kinnas, S., Abdel-Maksoud, M., Barkmann, U., Lubke, L. and Tian,Y. 2015: Proceedings of the Second Workshop on Cavitation an Propeller Performance, *The Fourth International Symposium on Marine Propulsors, SMP 2015*, Austin, Texas, USA.

McCormick Jr., B.W. 1962: On Cavitation Produced by a Vortex Trailing From a Lifting Surfaces. *Journal of Basic Engineering*.

Morino, L. and Kuo, C.C., 1974: Subsonic Potential Aerodynamics for Complex Configurations: a General Theory, *AIAA Journal* 12, pp.191-197.

Sauer, J. and Schnerr, G., 2000: Unsteady cavitating flows – a new cavitation model based on a modified front capturing method and bubble dynamics, *Proceedings of the 2000 ASME Fluid Engineering Summer Conference,* Boston, Massachusetts, USA.